Active Plasmonics: Surface Plasmon Interaction With Optical Emitters

Muralidhar Ambati, Dentcho A. Genov, Rupert F. Oulton, and Xiang Zhang

(Invited Paper)

***Abstract*—The interaction between surface plasmons and optical emitters is fundamentally important for engineering applications, especially surface plasmon amplification and controlled spontaneous emission. We investigate these phenomena in an active planar metal-film system comprising InGaN/GaN quantum wells and a silver film. First, we present a detailed study of the propagation and amplification of surface plasmon polaritons (SPPs) at visible frequencies. In doing so, we propose a multiple quantum well structure and present quantum well gain coefficient calculations accounting for SPP polarization, line broadening due to exciton damping, and particularly, the effects of finite temperature. Second, we show that the emission of an optical emitter into various channels (surface plasmons, lossy surface waves, and free radiation) can be precisely controlled by strategically positioning the emitters. Together, these could provide a range of photonic devices (for example, surface plasmon amplifiers, nanolasers, nanoemitters, plasmonic cavities) and a foundation for the study of cavity quantum electrodynamics associated with surface plasmons.**

***Index Terms*—Amplification, multiple quantum wells (MQWs), Purcell factor, spontaneous emission, surface plasmons.**

I. Introduction

SURFACE plasmon polaritons (SPPs) are surface-bound electromagnetic waves, coupled to electron density oscillations, guided along metal–dielectric interfaces [1]–[3]. The unique features of surface plasmons, namely enhanced and spatially confined fields, combined with advances in fabrication technologies has led to renewed interest in exploring plasmonics for various applications [4] ranging from nanolithography [5], microscopy [6]–[9], solar cells [10], and metamaterials [11]–[13] to bio-sensing [14] and plasmonic circuits [15]–[18]. However, the field enhancements and propagation distances associated with SPPs are limited due to intrinsic losses in metals [19]. The study of the interaction of surface plasmons with active media, commonly referred to as active plasmonics, offers possible solutions; the expansion of surface-plasmon-based applications [20]–[23] as well as the study of the emission characteristics of optical emitters in plasmonic systems [24]–[26] have been recurrent themes in recent literature.

In our first study of active plasmonics, we discuss surface plasmon amplification. Several schemes utilizing various metal geometries and active media have been proposed to achieve surface plasmon amplification. Gain-assisted SPP propagation has been studied in planar metallic films, strips, and gratings [27]–[30]. The effects of gain media on localized surface plasmons are also discussed with respect to random composite materials comprising metal particles and two-level emitters [31]–[33]. In addition to these theoretical works, some recent experiments have demonstrated SPP lasing at 10 μm wavelength [34], and the partial compensation of loss in localized surface plasmons [35] and SPPs at visible wavelengths [36]. However, experimental work on surface plasmon amplification at visible and infrared frequencies has not yielded the desired results in terms of the magnitude of amplification. Conquering surface plasmon losses imposes stringent requirements on the gain media. Colloidal quantum dots seem to be the most promising choice as they yield high-gain coefficients and are frequency tunable due to quantum confinement. However, the high nonradiative rates associated with colloidal quantum dots prove to be a hindrance; the stimulated emission rate should dominate in order to observe surface plasmon amplification [37], which is a work in progress [38]. In contrast, multiple quantum well (MQW) structures are well-established gain media for lasing applications [39], [40]. Here, we analyze a silver–InGaN/GaN system accounting for the various characteristics of SPPs and the gain media relevant to amplification: refractive index and polarization of SPP as well as line broadening due to exciton damping and Fermi population inversion factor. Here, the focus is on the temperature dependence of MQW gain; high temperatures lead to a reduction in material gain coefficients and are hence detrimental to surface plasmon amplification. Such types of analyses could prove to be extremely useful for designing SPP amplifiers and lasers.

Our second study examines the modification of emission characteristics of an optical emitter when placed in proximity to a metal film, which follows the legacy of numerous theoretical and experimental studies [41]–[45]. Although the spontaneous emission coupling to different SPP modes in various metal–dielectric geometries has been well studied, the relative coupling strengths to the SPP modes have remained elusive. Here, we present a systematic evaluation of the various emission channels from the spontaneous emission of an emitter, a radiating dipole, close to a metal film for GaN/InGaN semiconductor

Manuscript received December 2, 2007. Current version published December 24, 2008. This work was supported by the Air Force Office of Scientific Research Multi-University Research Initiative (AFOSR MURI) on plasmonics under Grant FA9550-04-1-0434 and by the National Science Foundation (NSF) Nanoscale Science and Technology Center (NSEC) under Award DMI-0327077.

The authors are with the Center of Scalable and Integrated Nano-Manufacturing (SINAM), Department of Mechanical Engineering, University of California, Berkeley, CA 94720 USA (e-mail: murli@berkeley.edu; dgenov@berkeley.edu; ruper@berkeley.edu; xiang@berkeley.edu).

Color versions of one or more of the figures in this paper are available online at http://ieeexplore.ieee.org.

Digital Object Identifier 10.1109/JSTQE.2008.931108

structure. In addition, we show that tremendous control over relative amounts of emission can be achieved by varying the metal film thickness as well as the distance between the emitter and the metal film. Therefore, the results presented here could be crucial in the design of nanoscale light emission devices.

Our paper is organized as follows. First, we briefly present the permittivity renormalization method and adapt it to visible frequencies. This technique is used to derive explicit solutions of SPP dispersion, propagation length, and the gain requirements to overcome the intrinsic SPP loss. Second, we propose a GaN/InGaN MQW structure for SPP amplification; we present the efficacy of the MQW structure for SPP amplification at low temperatures and room temperature. Finally, we analyze exciton–SPP coupling in a GaN/InGaN–silver film system to achieve spontaneous emission control.

II. Permittivity Renormalization Technique

In this section, we review the permittivity renormalization technique [27], which provides an effective method to study SPP characteristics analytically. SPPs are TM-polarized surface electromagnetic waves propagating along metal–dielectric interfaces and are direct solutions of Maxwell's equations. A metal film of finite thickness d in a symmetric dielectric environment supports two SPP modes, which are labeled according to the symmetry of the surface charge (tangential electric field) distribution, as shown in Fig. 1(a). The dispersion relation of these SPP modes $k_{s,a}(\omega)$ is implicit in nature. To provide explicit scaling laws, we use first-order approximations and introduce the concept of a quasi-metal. The quasi-metal permittivity $\bar{\varepsilon}_m^{s,a}(\omega, d)$ reduces both symmetric and asymmetric SPP modes to an equivalent SPP mode at an interface separating semi-infinite metal and dielectric, such that $k_{s,a}^2 = k_0^2 \varepsilon_d \bar{\varepsilon}_m^{s,a}/(\bar{\varepsilon}_m^{s,a} + \varepsilon_d)$, where $k_0 = \omega/c$ is the wave vector in free space. The dielectric host permittivity $\varepsilon_d = n^2(1 + i\Delta)$ is a complex function where $\Delta > 0$ corresponds to an active medium and $\Delta < 0$ to a dissipative medium. Introducing a new representation for the metal permittivity is indispensable in order to obtain versatile analytical expressions. The bulk metal permittivity is described by the Drude model $\varepsilon_m = n_b^2 - \omega_p^2/(\omega^2 - i\omega\omega_\tau)$, where n_b is the contribution due to bound electrons, ω_p is the plasma frequency, and ω_τ is the relaxation rate. In the case $\omega < \omega_p$, we write $\varepsilon_m = \varepsilon_m' + i\varepsilon_m'' = (-1 + i\kappa)/\varepsilon$, where $\varepsilon = 1/|\varepsilon_m'| \ll 1$ and $\kappa = \varepsilon_m''/|\varepsilon_m'| \ll 1$. The SPP wave vector k_{SP} and propagation length l_{SP} are given by

$$k_{\mathrm{SP}} = n_{\mathrm{SP}} k_0 \qquad l_{\mathrm{SP}} = k_{\mathrm{SP}}^{-1} \frac{1 - n^2\bar{\varepsilon}}{\Delta + n^2\bar{\kappa}\bar{\varepsilon}} \tag{1}$$

where $n_{\mathrm{SP}} = n/\sqrt{1 - n^2\bar{\varepsilon}} > n$ is the SPP index of refraction, and the mode-dependent quasi-metal permittivity $\bar{\varepsilon}_m = (-1 + i\bar{\kappa})/\bar{\varepsilon}$ is a function of the incident frequency and slab thickness

$$\bar{\varepsilon}_{s,a}(\omega, d) = \varepsilon \frac{1 + n^2\varepsilon}{r_{s,a} + n^2\varepsilon} \qquad \theta_s = r_s \qquad \theta_a = 1$$

$$\bar{\kappa}_{s,a}(\omega, d) = \frac{\kappa\varepsilon}{\bar{\varepsilon}_{s,a}} \frac{1 + \varphi_{s,a} + 2n^2\theta_{s,a}\varepsilon}{r_{s,a} + 2n^2\varepsilon}. \tag{2}$$

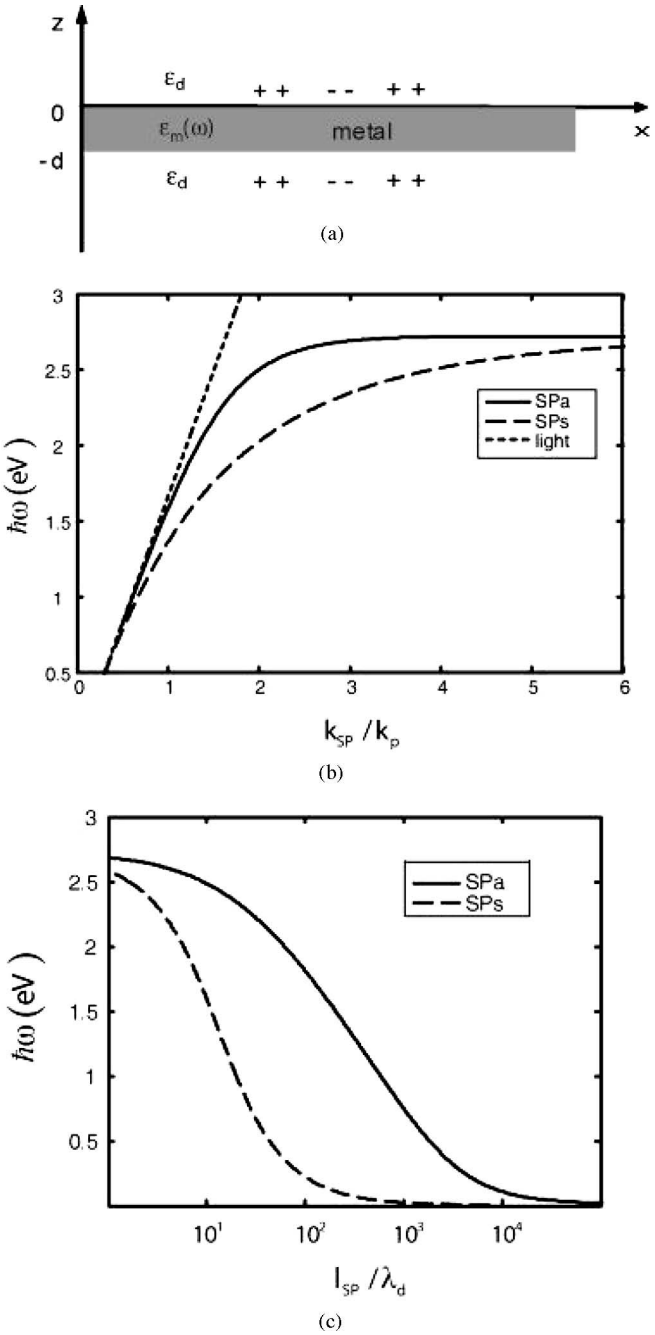

Fig. 1. (a) Charge distribution for a symmetric SPP mode in a thin metal film of thickness d and permittivity ε_m embedded in a dielectric host of permittivity ε_d. (b) ω–k_{SP} and (c) ω–l_{SP} plots for a silver–GaN system are calculated for the metal film with thickness $d = 30$ nm. In these calculations, we use silver with experimentally fitted parameters [63]: $\omega_p = 9.1$ eV, $\omega_\tau = 0.021$ eV, $n_b = 2.24$, and $\lambda_d = \lambda/n$ is the wavelength in the host media (GaN), $\varepsilon_d = 6$, and the SPP wave vector k_{SP} is normalized to the plasma wave vector.

The modal functions $r_s = 1/r_a = \tanh^2((1/2)d\Lambda)$ and $\varphi_s = -\varphi_a = (1/2)d\Lambda\,\mathrm{csch}((1/2)d\Lambda)\,\mathrm{sech}((1/2)d\Lambda)$ are frequency-dependent, since $\Lambda = k_p\sqrt{1 + n^2\varepsilon}$ ($k_p = \omega_p/c$) is the plasma wave vector. Note that the bulk metal properties are recovered in the thick film limit. In order to calculate the critical modal gain required to compensate intrinsic losses in the metal, we use (1) to seek a solution for Δ such that the propagation length diverges, $\Delta = \Delta_c^{s,a} = -n^2\bar{\varepsilon}_{s,a}\bar{\kappa}_{s,a}$. At low frequencies ($\varepsilon \ll 1$), critical

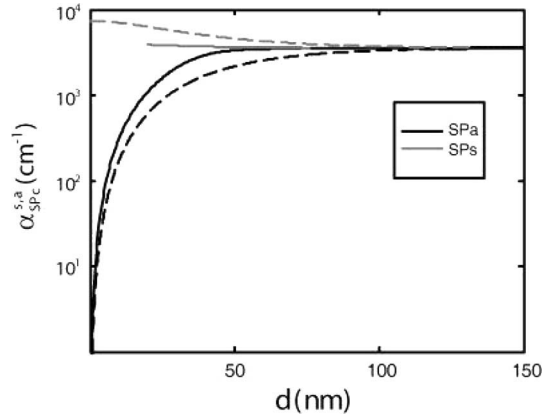

Fig. 2. Critical modal gain vs. metal film thickness d at $\lambda = 480$ nm, $\hbar\omega = 2.59$ eV. The exact solutions (solid lines), obtained numerically, for modal gain requirements are compared to the explicit analytical result (3) (dashed lines). The critical gain requirement has an asymptotic behavior with decreasing film thickness for the symmetric SPP (gray lines). The exact solution did not converge for very thin films. Since $\hbar\omega = 2.59$ eV is close to the SPP resonance, the critical modal gain for the symmetric SPP is very high. In contrast, the gain requirement sharply decreases with decreased metal film thickness for the asymmetric SPP mode (black lines).

gain reduces to

$$\Delta_c^{s,a} = \Delta_0 \frac{1 + \varphi_{s,a} + 2n^2\theta_{s,a}\omega^2/\omega_p^2}{r_{s,a} + 2n^2\omega^2/\omega_p^2} \tag{3}$$

where $\Delta_0 = -n^2\varepsilon\kappa \approx -n^2\omega\omega_\tau/\omega_p^2$ is the critical value for a single metal–dielectric interface.

The dispersion of the SPP wave vector and SPP propagation length for the silver–GaN system are shown in Fig. 1(b) and (c). Both the symmetric and asymmetric modes are displayed; the SPP branches asymptotically approach the SPP "resonance" at $\hbar\omega_{\rm SP} = 2.74$ eV. The propagation lengths [Fig. 1(c)] are limited near the SPP resonance and increase with decreasing frequency. In principle, a stronger decay of the long-range asymmetric SPP occurs due to alloy scattering events and carrier–carrier interactions in GaN. For simplicity, we neglect this effect in propagation length calculations; however, it is included in the gain calculations discussed in Section III. Fig. 2 displays the critical gain $\alpha_{{\rm SP}c}^{s,a} = -nk_0\,\Delta_c^{s,a}$ required at $\lambda = 480$ nm ($\hbar\omega = 2.59$ eV) to achieve an infinite SPP propagation length for a wide range of metal thickness. In thick films, the SPP modes are degenerate and a modal gain $\alpha_{{\rm SP}c}^{0} = -nk_0\,\Delta_0 = 3540$ cm^{-1} is sufficient to provide amplification. This high modal gain is required because the wavelength that we have chosen is close to the SPP resonance. For thin films, the symmetric SPP requires a higher modal gain than that for the asymmetric mode, which is expected as the symmetric SPP's energy concentration in the metal film is higher. In contrast to the symmetric mode, the critical modal gain decreases with decreasing film thickness for the asymmetric mode. Fig. 2 also displays the exact critical modal gain required, which agrees well with the approximate solutions generated using the permittivity renormalization technique. These explicit solutions provide important new insights since they highlight the different scaling laws; for example, in the case of thin films, it predicts that the critical gain for the asymmetric SPP mode diminishes quadratically with decreasing film thickness, $\lim_{d\to 0} nk_0|\Delta_c^a| = k_0 n^5 \kappa\varepsilon^2 k_p^2 d^2$. As the critical modal gain depends linearly on the metal loss, additional losses, due to surface roughness of thin metal films and electron-boundary scatterings, can be accounted through modification of the imaginary part of the metal permittivity $\kappa^{s,a}$. SPP-based transmission lines under asymmetric mode excitation look most promising for amplification as the critical modal gain requirements are less stringent.

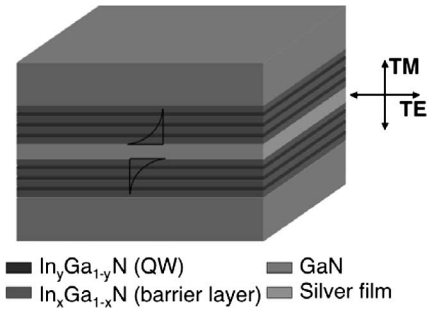

Fig. 3. InGaN/GaN: metal geometry for the study of SPP amplification. Silver metal film of finite thickness is surrounded by the QW heterostructures. The heterostructure consists of GaN, InGaN barrier layer ($x = 0.02$) of thickness 7 nm, and InGaN QW ($y = 0.2$) of thickness $w = 5$ nm. Schematic of SPP energy flux decaying exponentially away from the metal surface is shown in addition to TE and TM polarizations for the QW structure.

III. MQW System for Surface Plasmon Amplification

The review in the previous section identifies that SPP amplification, characterized by an infinite propagation length, could be achieved with a gain medium surrounding the metal film. We now consider an InGaN/GaN MQW structure with geometry typical of current devices on either sides of the metal film, as shown in Fig. 3. We report the effectiveness of this MQW structure for SPP amplification at $T = 0$ K and at low and ambient temperatures. We begin by evaluating the linear material gain α_m using time-dependent perturbation theory [46] accounting for carrier lifetime broadening γ due to alloy scattering, SPP index $n_{\rm SP}$, polarization, and additional line broadening due to finite temperatures and band occupation

$$\alpha_m(\hbar\omega) = C_{\rm SP}\int_0^\infty \rho_r^{2D} M \frac{(\gamma/\pi)[f_c(E) - f_v(E)]}{[E_h^e(0) + E - \hbar\omega]^2 + \gamma^2} dE. \tag{4}$$

Here, $C_{\rm SP} = e^2\pi/c\omega\varepsilon_0 n_{\rm SP} m_0^2$, with c being the speed of light in vacuum, ε_0 the permittivity of free space, m_0 the mass of an electron and e its charge, $\rho_r^{\rm 2D}$ is the reduced 2-D density of states, $M = |\hat{g}_{\rm SP}\cdot\vec{p}_{cv}|^2$ is the transition matrix element, $\hat{g}_{\rm SP} = \vec{A}_{\rm SP}/|\vec{A}_{\rm SP}|$ is a unit vector corresponding to the SPP vector potential accounting for the presence of SPP electromagnetic field, $\vec{p}_{cv}$ is the momentum vector, $E_e^h(0)$ is the energy corresponding to the transition from the bottom of first conduction subband to the top of first valence subband, and f_c and f_v are the Fermi–Dirac distributions for the electrons in the valence and conduction bands, respectively.

The Fermi–Dirac population inversion factor $f_c - f_v > 0$ introduces an additional line broadening due to the finite

temperature and band occupation. It is important to note that (4) differs from the gain in conventional laser systems in two ways: first, the material gain α_m is reduced by a factor $n/n_{\rm SP}$ as compared to unbound plane wave propagation in the MQW, and second, a decrease in peak gain is expected due to the SPP polarization, which, at low frequencies, is predominantly TM with respect to the quantum well (QW). SPP modes close to the light line are better served with tensile strained MQW structures for amplification studies, in which the transitions from first conduction subband to the first light-hole subband contribute to the gain. However, SPP modes have a strong longitudinal component (TE with respect to QW) at resonance. Compressively strained or unstrained QWs provide the optimum gain to these SPP modes by virtue of transitions from the first conduction subband to the first heavy-hole subband.

For compressively strained InGaN/GaN MQWs with small well sizes, only the $e1$–$hh1$ transition contributes to gain. The matrix element accounting for SPP propagation, which has electric fields along and perpendicular to the direction of SPP propagation, is reduced by polarization factor $\mu_{s,a} = (\Lambda_d^{s,a})^2/[k_{s,a}^2 + (\Lambda_d^{s,a})^2]$, where $\Lambda_d^{s,a} = {\rm Re}\sqrt{k_{s,a}^2 - \varepsilon_d k_0^2}$. Under operation far below saturation, we introduce the SPP modal gain $\alpha_{\rm SP} = -nk_0\Delta = \alpha_m\Phi - \alpha_{\rm abs}(1-\Phi)$, where $\alpha_{\rm abs}$ corresponds to absorption in the barrier layer. The electromagnetic confinement factor is given as $\Phi = \sum_i \int_{z_i}^{z_i+w} |S_x(\omega,z)|dz / \int_0^\infty |S_x(\omega,z)|dz$, where S_x is the time-averaged x-component of the SPP power flux, z_i is the position of the ith QW in relation to the metal slab, and w is its thickness. The confinement factor reduces to $\Phi_{s,a} = (1-e^{2w\Lambda_d^{s,a}})/(1-e^{2b\Lambda_d^{s,a}})$ for a periodic arrangement of the QWs with period b. It is vital to note that the dense packing of the MQW system close to the metal film favors higher modal gain. However, when decreasing the spacing between individual QWs and their overall distance from the metal film, a considerable decrease in performance could be expected due to enhanced spontaneous emission into lossy surface waves (LSWs) and reduced carrier confinement, respectively. The enhanced spontaneous emission into the various emission channels for this geometry is discussed in detail in Section IV.

For the study of SPP amplification associated with silver and InGaN/GaN heterostructures, it is better to work away from the SPP resonance, for example, in green spectral region. However, this spectral region requires indium-rich InGaN QWs. Though light emission devices have been developed with high indium composition ratios (>0.2), fluctuations in indium concentration can occur in these QWs; even a slight InGaN segregation may provide a hindrance to the mechanism of optical gain in nitrides and therefore laser diodes [47]–[49]. Here, we consider an InGaN QW structure, which has been used for a laser diode [50], and we modify the QW thickness such that the gain peak is close to 480 nm wavelength. For simplicity, we neglect the effect of temperature on the bandgaps of nitrides and the strain changes.

The SPP modal gain for InGaN/GaN MQW is calculated for both SPP modes at low ($T = 0$ K, $T = 77$ K) and ambient temperatures ($T = 300$ K) [Fig. 4(a) and (b)]. In these calculations, we set the characteristic parameters of the MQW as $w = 5$ nm and $b = 12$ nm, which define the transition frequency

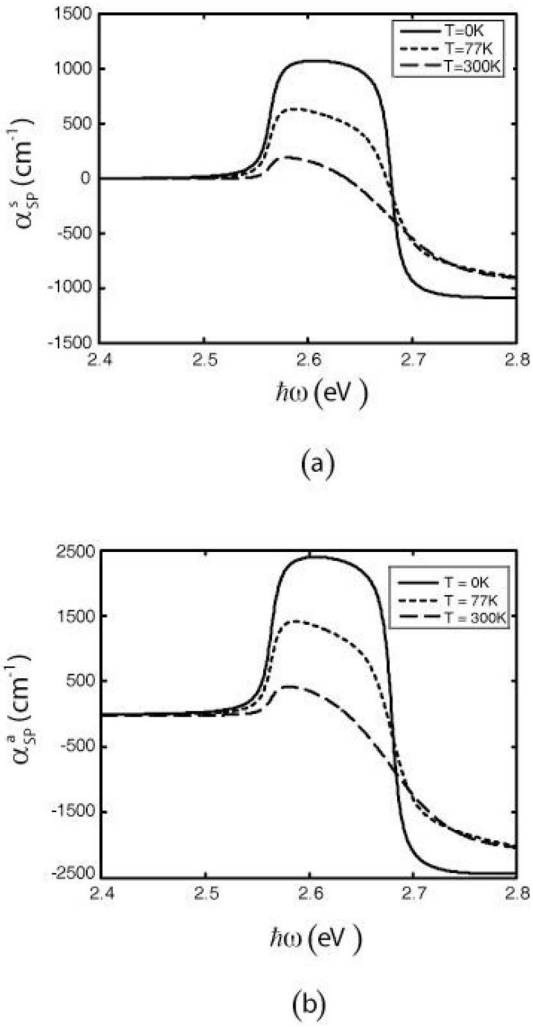

Fig. 4. SPP modal gains are calculated separately for both (a) symmetric and (b) asymmetric SPP modes as a function of $\hbar\omega$ with a fixed carrier density, $n = 1\times10^{19}$ cm^{-3}. In each of these plots, the temperature dependence is plotted for $T = 0$ K, liquid nitrogen temperature (77 K), and room temperature (300 K). It is clear that Fermi–Dirac factor at finite temperature reduces the peak gain and gain bandwidth with increasing temperatures. Considering a silver film of thickness $d = 30$ nm, SPP refractive index $n_{\rm SP}$ and modal factors Φ as well as polarization factors μ are accounted in these calculations: $n_{\rm SP}^s = 7.0$, $n_{\rm SP}^a = 3.45$, $\Phi_s = 0.19$, $\Phi_a = 0.3$, $\mu_s = 0.47$, and $\mu_a = 0.33$.

as $\hbar\omega_{e1\text{-}hh1} = 2.56$ eV and the exciton damping $\gamma \approx 7.3$ meV [51]– [54]. At low temperature, the injection current density required to maintain sheet carrier density $n_{2\rm D} = 5\times10^{12}$ cm^{-2} is $J \approx 10$ kA/cm^2. At this injection rate, the peak modal gain $\alpha_{\rm SP,max}^a = 2386$ cm^{-1} and $\alpha_{\rm SP,max}^s = 1066$ cm^{-1} are obtained for $T = 0$ K. The polarization-dependent QW gain coefficients $\mu_a < \mu_s$ combined with the electromagnetic confinement factors $\Phi_a > \Phi_s$ and SPP refractive index $n_{\rm SP}^a < n_{\rm SP}^s$ result in different peak modal gains for the symmetric and the asymmetric SPP (Fig. 4). In comparison to the critical SPP modal gain (Fig. 2), the calculated gain coefficients [Fig. 4(a)] clearly show that it is not possible, in principle, to overcome the losses associated with the symmetric SPPs. On the other hand, the modal gains obtained from the MQW structure are enough to compensate asymmetric SPP losses in thin films. The amplification

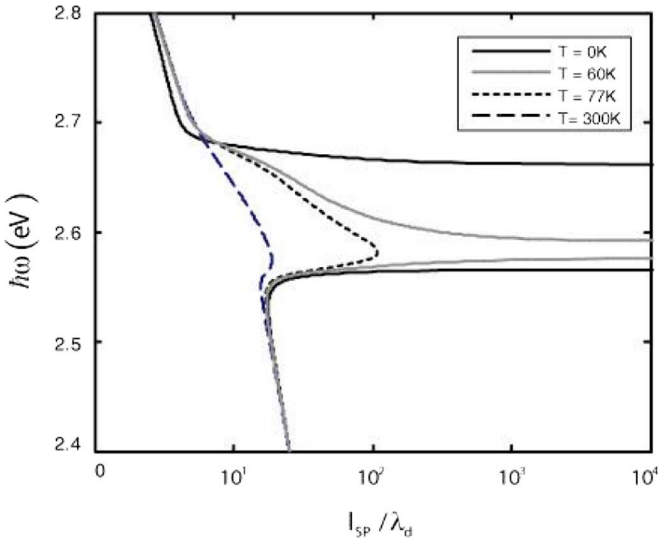

Fig. 5. ω–$l_{\rm SP}$ plot for the asymmetric SPP mode of the silver film $d = 30$ nm surrounded by MQW structure. The injection of carriers at different temperatures result in either complete compensation ($T = 0$ K and $T = 60$ K) or partial compensation ($T = 77$ K and higher) of SPP losses. The temperature $T = 60$ K is included to obtain the essence of the transition of temperature dependence on SPP amplification. The frequency amplification band decreases $\Delta\omega_a$ with the increase in temperature: $\Delta\omega_a = 0.1$ eV at $T = 0$ K, $\Delta\omega_a = 0.016$ eV at $T = 60$ K, and $\Delta\omega_a = 0$ at higher temperatures.

effects can be studied when SPPs interact with MQWs under population inversion, obtained by the injection of carriers. Further, this effect is observed only in narrow frequency bands around the transition frequency of the QW. The frequency amplification band $\Delta\omega_{s,a}$ over which the SPP attenuation is compensated depends on the intrinsic metal loss, SPP mode symmetry, carrier injection rate, and temperature. In addition, the SPP amplification bands reduce with increasing temperature because of decreased magnitude of SPP modal gains, which, in turn, is due to lower Fermi–Dirac factors for a given carrier injection. The temperature effect on SPP amplification is clearly shown in Fig. 5. An apparent way to reduce the asymmetric SPP losses and obtain wider amplification bands is to reduce the metal thickness. In such thin films, the asymmetric SPP mode is very sensitive to refractive index mismatches on either sides of the film, giving rise to another radiative loss mechanism to compensate.

The study so far has focused on the compensation of SPP losses using QW gain. We have shown that an InGaN/GaN MQW system can compensate the losses of the asymmetric SPP of a silver film; however, the effect of competition for emission with its symmetric counterpart is currently unclear. The symmetric and asymmetric SPPs' energy flows in sheets of thickness $t_{s,a} = 1/2\Lambda_d^{s,a}$, which overlap. The probability of emission into the asymmetric SPP, spontaneous emission factor, depends not only on the QW position relative to the silver film surface but also on the relative coupling strengths of the two SPPs. In fact, the population inversion can be depleted by enhanced spontaneous emission into any of the two SPPs, free-space (or radiation) modes, and a variety of nonradiative channels [55]. While the gain requirement for achieving loss compensation remains fixed, the asymmetric SPP's spontaneous emission factor determines the carrier injection rate necessary to maintain the same carrier concentration when the set of addition emission channels are incorporated into the model. This multiemission channel, enhanced exciton relaxation, near the metal is discussed in the next section.

IV. Controlled Spontaneous Emission

The modification of the spontaneous emission of an emitter located near a metallic film is due to the change in local density of states associated with surface plasmons. The Purcell factor $F_p \propto Q/V_m$ quantifies the modification of an emitter's emission rate relative to its free-space rate [56]. Although an enhancement is achievable by high Q cavity and the reduction of mode volume V_m, the focus here is on the latter, which is afforded by SPP field confinement. Even without a resonant cavity, SPPs have confined field distributions that provide high Purcell factors, which can lead to preferential coupling to specific emission channels [57]. When multiple SPPs compete for spontaneous emission, our study shows that the more confined modes are preferential. Furthermore, by localizing emitters at different distances from a metallic film, the relative amounts of emission into the SPPs can be controlled.

In this section, we evaluate the various emission channels from the spontaneous emission of an optical emitter close to a metal slab. An emitter in an excited state close to a metal slab spontaneously decays to the ground state by coupling to one of two SPPs, bulk radiation, or to LSWs. We examine this process for the InGaN/GaN semiconductor material system, at the emission wavelength $\lambda = 480$ nm. The emitter is modeled by a dipole situated at $x = y = 0$, $z = D$ next to a silver slab of thickness d and permittivity ε_m, embedded in a host dielectric of permittivity $\varepsilon_d = 6$, as shown in Fig. 6(a). The orientation of the dipole will be expressed in terms of the three orthogonal directions x, y, and z, where the first two are referred to as parallel dipoles ($\|$) and the other as the perpendicular dipole ($\perp$). The dipole experiences self-forcing reflections $r_\nu(u)$ as a result of coupling to TE ($\nu = s$) or TM ($\nu = p$) propagating and evanescent fields. The in-plane wave vector parameter u is normalized to the wavenumber and refractive index of the dielectric medium such that $k_r = \sqrt{\varepsilon_d}uk_0$, $k_{zd}^2 = -\Lambda_d^2 = \varepsilon_d(1-u^2)k_0^2$, and $k_{zm}^2 = -\Lambda_{zm}^2 = (\varepsilon_m - u^2\varepsilon_d)k_0^2$.

The radiative, $\Gamma_{R\mu}$, and nonradiative, $\Gamma_{{\rm NR}\mu}$, emission rates for a $\mu = \{\perp, \|\}$ oriented dipole relative to the free-space rate γ_0 are [58], [59]

$$\frac{\Gamma_{R\mu}(D,d)}{\gamma_0} = q\left(1 + \frac{3}{2}\,{\rm Im}\int_0^1 I_\mu(u,D,d)\frac{k_r}{k_{zd}}du\right)$$
$$\frac{\Gamma_{{\rm NR}\mu}(D,d)}{\gamma_0} = 1 - q\left(1 + \frac{3}{2}\,{\rm Im}\int_1^\infty I_\mu(u,D,d)\frac{k_r}{k_{zd}}du\right) \quad (5)$$

and $\gamma_\mu(D,d) = \Gamma_{R\mu}(D,d) + \Gamma_{{\rm NR}\mu}(D,d)$ is the total modified emission rate. Here, q is the light–matter conversion quantum efficiency and the integrands $I_\mu(u)$ are

$$I_\perp(u,D,d) = r_p(u,d)u^2\,\exp(-2\Lambda_d D)$$
$$I_\|(u,D,d) = \frac{1}{2}(r_s(u,d)u^2 + r_p(u,d)(1-u^2))\exp(-2\Lambda_d D) \quad (6)$$

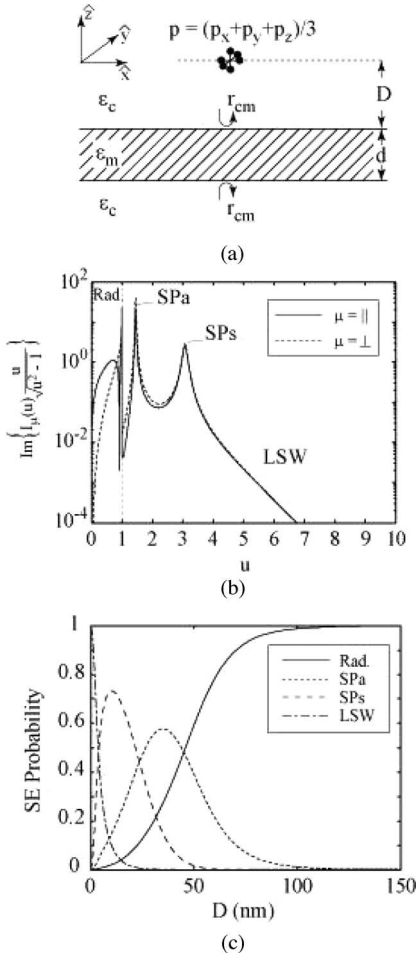

Fig. 6. (a) Schematic of dipole emitter at a distance D from a planar metal slab of thickness d. (b) Evaluation of the integrand in (5) for $D = 10$ nm, $d = 30$ nm, and $\lambda = 480$ nm. This highlights contributions to the emission rate from bulk radiation, asymmetric/symmetric SPPs, and LSWs. (c) Spontaneous emission probabilities into the various emission channels as a function of D for $d = 30$ nm.

and $r_\nu(u)$ are the Fresnel reflection coefficients for the dielectric–metal–dielectric system

$$r_\nu(u,d) = \frac{r_{dm(\nu)}(u)(\exp(2\Lambda_m d) - 1)}{1 - r^2_{dm(\nu)}(u)\exp(2\Lambda_m d)} \tag{7}$$

where $r_{dm(\nu)}(u)$ are the Fresnel reflection coefficients for the ν polarization at the GaN–silver interface. The lifetimes for emission into the coupled SPP modes requires the evaluation of two further integrals; these will be expressed as complex contour integrals around the poles of the integrand $u_i (i = \{s, a\})$ due to the symmetric and asymmetric SPP modes, respectively. The positions of the poles are identified through the p-polarization reflection coefficient $r_p(u) \to \infty$ such that $r^2_{dm(\nu)} = \exp(-2\Lambda_m d)$. The complex locations of the reflection poles are calculated using an integral approach [60], [61].

Fig. 6(b) shows the angular emission distribution at $\lambda = 480$ nm for a dipole embedded in GaN, $\varepsilon_d = 6$, situated at $D = 10$ nm from a flat silver slab of thickness $d = 30$ nm. Four emission channels are identified: radiation modes exist below the light line in GaN; two coupled SPP modes are identified by their resonant behavior from the reflection poles; and the remaining nonradiative proportion is identified as LSWs [55]. The radiative portion corresponds directly to the integral in (5) over the propagation band ($u = [0, 1]$). The remaining integral ($u = [1, \infty]$) providing the nonradiative components can be deconvolved further by evaluating the integral contributions in the vicinity of the SPP reflection poles. It follows that the emission rate for LSWs $\Gamma_{\mathrm{LSW}\mu} = \Gamma_{\mathrm{NR}\mu} - \Gamma^a_{\mathrm{SPP}\mu} - \Gamma^s_{\mathrm{SPP}\mu}$, where

$$\frac{\Gamma^{s,a}_{\mathrm{SPP}\,\mu}}{\gamma_0} = 1 - q\left(1 + \frac{3}{2}\,\mathrm{Im}\oint_{C_{s,a}} I_\mu(u,d)\frac{k_r}{\Lambda_d}du\right). \tag{8}$$

The current study examines the emission rates for random dipole orientations corresponding to two-thirds $\parallel$ dipoles and one-third $\perp$ dipoles. However, the dipole orientation can have a significant impact on surface plasmon coupling efficiency; for instance, perpendicular dipoles suited to QWs under tensile strain couple most strongly to the near field and have a greater range of influence with respect to D. The averaged emission rates pertaining to radiation ($\overline{\Gamma}_R$), SPPs ($\overline{\Gamma}^{s,a}_{\mathrm{SPP}}$), and LSWs ($\overline{\Gamma}_{\mathrm{LSW}}$) are evaluated numerically where the total emission rate $\overline{\gamma}$ is the sum over all of the partial rates. The partial rates are a direct measure of the dipole–optical coupling strength of a particular emission channel. For example, the ratio of the asymmetric SPP rate and the total rate gives the emission probability into that mode. Following this prescription, the probabilities of emission into the four channels are calculated and shown in Fig. 6(c) as a function of the dipole position D for the same parameters as in the calculation of Fig. 6(b). Apparently, none of the potentially useful modes can compete with LSWs; emitters positioned within 5 nm of a metallic surface are completely quenched. Since the emission rate into a mode is inversely proportional to its modal volume, the majority of the emission couples to symmetric SPP mode under optimum conditions. The highly confined field distribution and LSW quenching defines the probability response that peaks nearer to the metal's surface than the asymmetric SPP mode. Most of the asymmetric SPP mode's field exists outside the metal leading to a reduced spontaneous emission rate with respect to its counterpart close to the metal surface. However, the asymmetric mode has limited influence away from the surface near the first antinode of the radiation modes. Bulk radiation becomes dominant only beyond the influence of near-field effects associated with SPPs and LSWs, and when the first antinode of the radiation field distribution is reached near $\lambda/4\sqrt{\varepsilon_d} \approx 50$ nm.

To further illustrate the competition between the SPP modes, the emission probabilities of symmetric and asymmetric SPPs are shown in Fig. 7(a) as a function of both the slab thickness d and emitter position D. The optimal emitter positions $D_s(d)$ and $D_a(d)$, and peak emission probabilities $\overline{\Gamma}^s_{\mathrm{SPP}}(D_s(d))/\overline{\gamma}$ and $\overline{\Gamma}^a_{\mathrm{SPP}}(D_a(d))/\overline{\gamma}$ are shown as projections on the base and left faces of the 3-D graph, respectively. The metal slab thickness controls the coupling between the underlying SPPs of the two metal–dielectric interfaces, and consequently, the relative degrees of confinement of the asymmetric and symmetric coupled SPPs. For thick films, the emission probabilities converge to the case for a single interface. Here, the asymmetric and

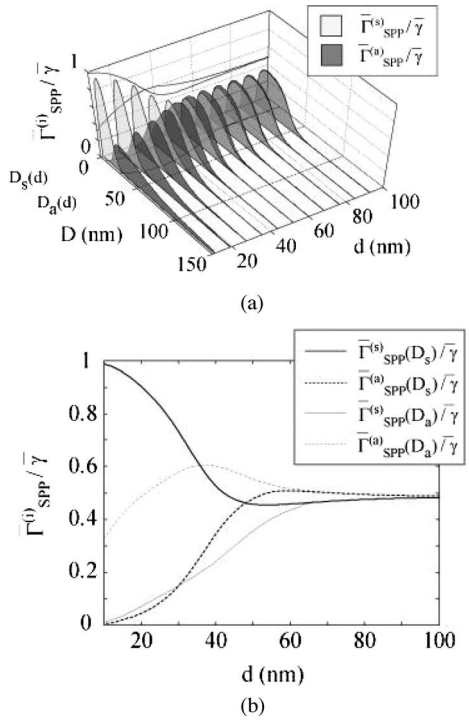

Fig. 7. (a) Transparent slices in this 3-D graph show the emission probabilities for symmetric (light gray) and asymmetric (dark gray) SPPs. The maximum probability for each SPP is projected onto the left-hand axis, while the positions of these peak values are projected onto the base. (b) Two cases where the emitters are positioned for either optimal coupling to symmetric (solid lines) or asymmetric (broken lines) SPPs.

symmetric modes become degenerate and the overall coupling to the single-surface SPP mode approaches about 84%. In the case of thin films, the coupled mode dispersion is strongest and the symmetric SPP takes almost ∼100% of the emission. In addition, the peak response of the symmetric mode shifts to smaller dipole positions (D) due to a combination of both reduced LSW emission rate and increased symmetric SPP emission rate.

The apparent spatial splitting of the optimum emitter position [$D_s(d)$ and $D_a(d)$] for the two SPP emission channels suggests that specific emitter localization can lead to effective mode discrimination. For instance, in the design of a nanoemitter device, it would be relevant to consider optimal coupling to one of the SPP emission channels. Fig. 7(b) shows the SPP emission probabilities for these two choices: heavy lines correspond to emitter localization at the peak of the symmetric SPP at $D_s(d)$ and light lines to that of the asymmetric SPP at $D_a(d)$. It may be noted that tuning to the symmetric SPP results in almost complete suppression of the asymmetric SPP for small D. On the other hand, tuning to the asymmetric SPP produces, at most, a 60% coupling with moderate suppression of the symmetric SSP (20%) for small d. Ultimately, the coupling to the asymmetric SPP is limited through competition with radiation modes. Though $\perp$ dipoles improve the overall coupling to SPPs for all d, there is no significant change compared to the general trends observed for averaged dipoles.

When considering geometries for SPP-based nanoscale light emitters and lasers, it is crucial to characterize all possible emission modes; although high spontaneous emission rates are available for SPP modes with small modal volumes, these modes are also naturally associated with high intrinsic propagation losses. However, the optimal coupling of the asymmetric SPP mode to a suitably strained QW may lead to low-threshold SPP lasers; here, the low threshold is in terms of carrier density but not necessarily the injection rates. This effect of low-threshold carrier concentration to realize the same gain coefficients for SPP amplification will be addressed elsewhere.

V. Conclusion

Active plasmonics has been rapidly expanding on both theoretical and experimental fronts. Experimental studies confirming SPP amplification by stimulated emission [36] and the generation of single SPPs [62] are the first major steps toward realizing quantum engineering associated with surface plasmons. Our analysis confirmed that a promising way to achieve SPP lasing at optical frequencies is by utilizing the asymmetric SPP mode of a thin metal slab at low temperatures with a symmetric dielectric environment for which MQW heterostructures comprising tensile strained QWs are perfect as the gain material. Current QW technology is capable of compensating intrinsic surface plasmon attenuation even near the plasmon resonance. However, this capability extends only to those SPP modes that are not excessively confined, such as the asymmetric SPP in the current study. In addition, the controlled spontaneous emission allows us to achieve efficient coupling to the desired asymmetric SPP mode. It is clear that in engineering new active plasmonic systems, careful consideration of the range of emission channels is important as spatial localization of the emission provides the ability to discriminate between unwanted emission modes and thereby reduce the threshold conditions for SPP lasing.

Another fundamental study in active plasmonics, which is not addressed in this paper, involves the strong coupling of SPPs and excitons. This phenomenon is realized when the maximum coupling strength between the emitter and SPP is larger than the decay rate of the excited state of the emitter and SPP decay rate. Such a phenomenon has been observed with an organic semiconductor, cyanine dye J-aggregate, and silver film where the collective coupling satisfies the necessary condition [25]. The strong coupling of a single exciton to a single SPP mode could be striking, and it may further open a route to new studies and experiments with exciton–surface plasmon interface.

References

[1] H. Raether, *Surface Plasmons on Smooth and Rough Surfaces and on Gratings*. Berlin, Germany: Springer-Verlag, 1988.
[2] R. H. Ritchie, "Plasma losses by fast electrons in thin films," *Phys. Rev.*, vol. 1, pp. 874–881, 1957.
[3] E. N. Economou, "Surface plasmons in thin films," *Phys. Rev.*, vol. 182, pp. 539–554, 1969.
[4] W. L. Barnes, A. Dereux, and T. W. Ebbesen, "Surface plasmon subwavelength optics," *Nature*, vol. 424, pp. 824–830, 2003.
[5] W. Srituravanich, N. Fang, C. Sun, Q. Luo, and X. Zhang, "Plasmonic nanolithography," *Nano Lett.*, vol. 4, pp. 1085–1088, 2004.
[6] N. Fang, H. Lee, C. Sun, and X. Zhang, "Sub-diffraction-limited optical imaging with a silver superlens," *Science*, vol. 308, pp. 534–537, 2005.
[7] Z. W. Liu, H. Lee, Y. Xiong, C. Sun, and X. Zhang, "Far-field optical hyperlens magnifying sub-diffraction-limited objects," *Science*, vol. 315, p. 1686, 1686.

[8] J. B. Pendry, "Negative refraction makes a perfect lens," *Phys. Rev. Lett.*, vol. 85, pp. 3966–3969, 2000.

[9] I. I. Smolyaninov, Y. J. Hung, and C. C. Davis, "Magnifying superlens in the visible frequency range," *Science*, vol. 315, pp. 1699–1701, 2007.

[10] P. Andrew, S. C. Kitson, and W. L. Barnes, "Surface-plasmon energy gaps and photoabsorption," *J. Mod. Opt.*, vol. 44, pp. 395–406, 1997.

[11] V. M. Shalaev, "Optical negative-index metamaterials," *Nat. Photon.*, vol. 1, pp. 41–48, 2007.

[12] V. P. Safonov, V. M. Shalaev, V. A. Markel, Y. E. Danilova, N. N. Lepeshkin, W. Kim, S. G. Rautian, and R. L. Armstrong, "Spectral dependence of selective photomodification in fractal aggregates of colloidal particles," *Phys. Rev. Lett.*, vol. 80, pp. 1102–1105, 1998.

[13] D. R. Smith, J. B. Pendry, and M. C. K. Wiltshire, "Metamaterials and negative refractive index," *Science*, vol. 305, pp. 788–792, 2004.

[14] K. Kneipp, Y. Wang, H. Kneipp, L. T. Perelman, I. Itzkan, R. Dasari, and M. S. Feld, "Single molecule detection using surface-enhanced Raman scattering (SERS)," *Phys. Rev. Lett.*, vol. 78, pp. 1667–1670, 1997.

[15] S. I. Bozhevolnyi, J. Erland, K. Leosson, P. M. W. Skovgaard, and J. M. Hvam, "Waveguiding in surface plasmon polariton band gap structures," *Phys. Rev. Lett.*, vol. 86, pp. 3008–3011, 2001.

[16] H. Ditlbacher, J. R. Krenn, G. Schider, A. Leitner, and F. R. Aussenegg, "Two-dimensional optics with surface plasmon polaritons," *Appl. Phys. Lett.*, vol. 81, pp. 1762–1764, 2002.

[17] S. A. Maier, "Plasmonics: Metal nanostructures for subwavelength photonic devices," *IEEE J. Sel. Topics Quantum Electron.*, vol. 12, no. 6, pp. 1214–1220, Nov./Dec. 2006.

[18] J. A. Dionne, L. A. Sweatlock, H. A. Atwater, and A. Polman, "Plasmon slot waveguides: Towards chip-scale propagation with subwavelength-scale localization," *Phys. Rev. B*, vol. 73, pp. 035407-1–035407-9, 2006.

[19] J. J. Burke, G. I. Stegeman, and T. Tamir, "Surface-polariton-like waves guided by thin, lossy metal-films," *Phys. Rev. B*, vol. 33, pp. 5186–5201, 1986.

[20] D. Pacifici, H. J. Lezec, and H. A. Atwater, "All-optical modulation by plasmonic excitation of CdSe quantum dots," *Nat. Photon.*, vol. 1, pp. 402–406, 2007.

[21] J. G. Rivas, M. Kuttge, H. Kurz, P. H. Bolivar, and J. A. Sanchez-Gil, "Low-frequency active surface plasmon optics on semiconductors," *Appl. Phys. Lett.*, vol. 88, pp. 082106-1–082106-3, 2006.

[22] A. V. Krasavin and N. I. Zheludev, "Active plasmonics: Controlling signals in Au/Ga waveguide using nanoscale structural transformations," *Appl. Phys. Lett.*, vol. 84, pp. 1416–1418, 2004.

[23] S. A. Ramakrishna and J. B. Pendry, "Removal of absorption and increase in resolution in a near-field lens via optical gain," *Phys. Rev. B*, vol. 67, pp. 201101-1–201101-4, 2003.

[24] D. E. Chang, A. S. Sorensen, P. R. Hemmer, and M. D. Lukin, "Quantum optics with surface plasmons," *Phys. Rev. Lett.*, vol. 97, pp. 053002-1–053002-11, 2006.

[25] J. Bellessa, C. Bonnand, J. C. Plenet, and J. Mugnier, "Strong coupling between surface plasmons and excitons in an organic semiconductor," *Phys. Rev. Lett.*, vol. 93, pp. 036404-1–036404-4, 2004.

[26] A. Neogi, C. W. Lee, H. O. Everitt, T. Kuroda, A. Tackeuchi, and E. Yablonovitch, "Enhancement of spontaneous recombination rate in a quantum well by resonant surface plasmon coupling," *Phys. Rev. B*, vol. 66, pp. 153305-1–153305-4, 2002.

[27] D. A. Genov, M. Ambati, and X. Zhang, "Surface plasmon amplification in planar metal films," *IEEE J. Quantum Electron.*, vol. 43, no. 11, pp. 1104–1108, Nov. 2007.

[28] M. Z. Alam, J. Meier, J. S. Aitchison, and M. Mojahedi, "Gain assisted surface plasmon polariton in quantum wells structures," *Opt. Exp.*, vol. 15, pp. 176–182, 2007.

[29] I. Avrutsky, "Surface plasmons at nanoscale relief gratings between a metal and a dielectric medium with optical gain," *Phys. Rev. B*, vol. 70, pp. 155416-1–155416-6, 2004.

[30] M. P. Nezhad, K. Tetz, and Y. Fainman, "Gain assisted propagation of surface plasmon polaritons on planar metallic waveguides," *Opt. Exp.*, vol. 12, pp. 4072–4079, 2004.

[31] D. J. Bergman and M. I. Stockman, "Surface plasmon amplification by stimulated emission of radiation: Quantum generation of coherent surface plasmons in nanosystems," *Phys. Rev. Lett.*, vol. 90, pp. 027402-1–027402-4, 2003.

[32] D. S. Citrin, "Plasmon-polariton transport in metal-nanoparticle chains embedded in a gain medium," *Opt. Lett.*, vol. 31, pp. 98–100, 2006.

[33] N. M. Lawandy, "Localized surface plasmon singularities in amplifying media," *Appl. Phys. Lett.*, vol. 85, pp. 5040–5042, 2004.

[34] A. Tredicucci, C. Gmachl, F. Capasso, A. L. Hutchinson, D. L. Sivco, and A. Y. Cho, "Single-mode surface-plasmon laser," *Appl. Phys. Lett.*, vol. 76, pp. 2164–2166, 2000.

[35] M. A. Noginov, G. Zhu, M. Bahoura, J. Adegoke, C. E. Small, B. A. Ritzo, V. P. Drachev, and V. M. Shalaev, "Enhancement of surface plasmons in an Ag aggregate by optical gain in a dielectric medium," *Opt. Lett.*, vol. 31, pp. 3022–3024, 2006.

[36] J. Seidel, S. Grafstrom, and L. Eng, "Stimulated emission of surface plasmons at the interface between a silver film and an optically pumped dye solution," *Phys. Rev. Lett.*, vol. 94, pp. 177401-1–177401-4, 2005.

[37] V. I. Klimov, A. A. Mikhailovsky, S. Xu, A. Malko, J. A. Hollingsworth, C. A. Leatherdale, H. J. Eisler, and M. G. Bawendi, "Optical gain and stimulated emission in nanocrystal quantum dots," *Science*, vol. 290, pp. 314–317, 2000.

[38] V. I. Klimov, S. A. Ivanov, J. Nanda, M. Achermann, I. Bezel, J. A. McGuire, and A. Piryatinski, "Single-exciton optical gain in semiconductor nanocrystals," *Nature*, vol. 447, pp. 441–446, 2007.

[39] B. Monemar and G. Pozina, "Group III-nitride based hetero and quantum structures," *Progr. Quantum Electron.*, vol. 24, no. 6, pp. 239–290, 2000.

[40] N. Holonyak, R. M. Kolbas, R. D. Dupuis, and P. D. Dapkus, "Quantum-well heterostructure lasers," *IEEE J. Quantum Electron.*, vol. QE-16, no. 2, pp. 170–186, Feb. 1980.

[41] I. Pockrand, A. Brillante, and D. Mobius, "Exciton surface-plasmon coupling—An experimental investigation," *J. Chem. Phys.*, vol. 77, pp. 6289–6295, 1982.

[42] J. Vuckovic, M. Loncar, and A. Scherer, "Surface plasmon enhanced light-emitting diode," *IEEE J. Quantum Electron.*, vol. 36, no. 10, pp. 1131–1144, Oct. 2000.

[43] P. T. Worthing, R. M. Amos, and W. L. Barnes, "Modification of the spontaneous emission rate of Eu3+ ions embedded within a dielectric layer above a silver mirror," *Phys. Rev. A*, vol. 59, pp. 865–872, 1999.

[44] C. F. Eagen, W. H. Weber, S. L. McCarthy, and R. W. Terhune, "Time-dependent decay of surface-plasmon-coupled molecular fluorescence," *Chem. Phys. Lett.*, vol. 75, pp. 274–277, 1980.

[45] H. Morawitz and M. R. Philpott, "Coupling of an excited molecule to surface plasmons," *Phys. Rev. B*, vol. 10, pp. 4863–4868, 1974.

[46] S. L. Chuang, *Physics of Optoelectronic Devices*. New York: Wiley, 1995.

[47] D. P. Bour, M. Kneissl, L. T. Romano, M. D. McCluskey, C. G. Van deWalle, B. S. Krusor, R. M. Donaldson, J. Walker, C. J. Dunnrowicz, and N. M. Johnson, "Characteristics of InGaN–AlGaN multiple-quantum-well laser diodes," *IEEE J. Sel. Topics Quantum Electron.*, vol. 4, no. 3, pp. 498–504, May/Jun. 1998.

[48] S. Chichibu, T. Azuhata, T. Sota, and S. Nakamura, "Luminescences from localized states in InGaN epilayers," *Appl. Phys. Lett.*, vol. 70, pp. 2822–2824, 1997.

[49] S. Nakamura, "The roles of structural imperfections in InGaN-based blue light-emitting diodes and laser diodes," *Science*, vol. 281, pp. 956–961, 1998.

[50] K. Kojima, M. Funato, Y. Kawakami, S. Nagahama, T. Mukai, H. Braun, and U. T. Schwarz, "Gain suppression phenomena observed in $In_xGa_{1-x}N$ quantum well laser diodes emitting at 470 nm," *Appl. Phys. Lett.*, vol. 89, pp. 241127-1–241127-3, 2006.

[51] M. Goano, E. Bellotti, E. Ghillino, C. Garetto, G. Ghione, and K. F. Brennan, "Band structure nonlocal pseudopotential calculation of the III-nitride wurtzite phase materials system. Part II. Ternary alloys $Al_xGa_{1-x}N$, $In_xGa_{1-x}N$, and $In_xAl_{1-x}N$," *J. Appl. Phys.*, vol. 88, pp. 6476–6482, 2000.

[52] H. Haag, P. Gilliot, R. Levy, B. Honerlage, O. Briot, S. Ruffenach-Clur, and R. L. Aulombard, "Excitonic absorption of GaN epilayers on sapphire: Dynamics, intensity, and temperature dependence," *Phys. Rev. B*, vol. 59, pp. 2254–2260, 1999.

[53] Y. C. Yeo, T. C. Chong, M. F. Li, and W. J. Fan, "Analysis of optical gain and threshold current density of wurtzite InGaN/GaN/AlGaN quantum well lasers," *J. Appl. Phys.*, vol. 84, pp. 1813–1819, 1998.

[54] J. W. Orton and C. T. Foxon, "Group III nitride semiconductors for short wavelength light-emitting devices," *Rep. Progr. Phys.*, vol. 61, pp. 1–75, 1998.

[55] G. W. Ford and W. H. Weber, "Electromagnetic-interactions of molecules with metal-surfaces," *Phys. Rep., Rev. Sect. Phys. Lett.*, vol. 113, pp. 195–287, 1984.

[56] E. M. Purcell, "Spontaneous emission probabilities at radio frequencies," *Phys. Rev.*, vol. 69, p. 681, 1946.

[57] R. W. Gruhlke, W. R. Holland, and D. G. Hall, "Optical-emission from coupled surface-plasmons," *Opt. Lett.*, vol. 12, pp. 364–366, 1987.

[58] R. R. Chance, A. Prock, and R. Silbey, "Molecular fluorescence and energy transfer near interfaces," *Adv. Chem. Phys.*, vol. 37, pp. 1–65, 1978.
[59] A. Sommerfeld, *Partial Differential Equations in Physics*. New York: Academic, 1949.
[60] E. Anemogiannis, E. N. Glytsis, and T. K. Gaylord, "Efficient solution of eigenvalue equations of optical wave-guiding structures," *J. Lightw. Technol.*, vol. 12, no. 12, pp. 2080–2084, Dec. 1994.
[61] A. A. Romanenko and A. B. Sotskii, "Solution of dispersion relations for planar waveguides in the case of complex roots," *Tech. Phys.*, vol. 43, pp. 427–433, 1998.
[62] A. V. Akimov, A. Mukherjee, C. L. Yu, D. E. Chang, A. S. Zibrov, P. R. Hemmer, H. Park, and M. D. Lukin, "Generation of single optical plasmons in metallic nanowires coupled to quantum dots," *Nature*, vol. 450, pp. 402–406, 2007.
[63] E. D. Palik, *Handbook of Optical Constants of Solids*. New York: Academic, 1985.

Muralidhar Ambati received the B.Tech. degree from Indian Institute of Technology, Chennai, India, and the M.S. degree from Texas A& M University, College Station. He is currently working toward the Ph.D. degree at the Department of Mechanical Engineering, University of California, Berkeley.

His current research interests include metamaterials and plasmonics.

Mr. Ambati is a member of the International Society for Optical Engineering (SPIE), the American Physical Society (APS), and the Materials Research Society (MRS). He was a recipient of the MRS Graduate Student Award as well as the Royce E. Wisenbaker'39 Graduate Fellowship and the Forsythe Graduate Fellowship at Texas A& M University.

Dentcho A. Genov received the equivalent of a European M.S. degree in nuclear physics from Sofia University, Sofia, Bulgaria, in 1999, the M.S. degree in optical physics (with a minor in computer science) from New Mexico State University, Las Cruces, in 2001, and the Ph.D. degree in electrical and computer engineering and the M.S.A.A. degree in aeronautics and astronautics from Purdue University, West Lafayette, IN, in 2005.

In 2005, he joined the National Science Foundation (NSF) Nanoscale Science and Engineering Center, University of California, Berkeley, as a Postdoctoral Research Associate. His current research interests include plasma physics and theoretical electrodynamics. He developed a numerical package for Monte Carlo simulations of an actual plasma focus device (PF-1000), and introduced highly efficient numerical and analytical methods for solving complex problems of electromagnetic wave interactions at the nanoscale. He is the author or coauthor of two book chapters and more than 30 papers published in leading peer-reviewed journals and conference proceedings.

Dr. Genov is a member of the Optical Society of America (OSA), the International Society for Optical Engineering (SPIE), and the American Physical Society (APS).

Rupert F. Oulton received the M.Sc. degree and the Ph.D. degree in physics from Imperial College, London, U.K., in 1997 and 2001, respectively.

At the Imperial College, he worked on inorganic and organic semiconductor optical devices including resonant cavity LEDs for free-space optical interconnects and post-microcavities as efficient single-photon sources for quantum cryptography. From 2003 to 2005, he was with Mitsubishi Corporation, where he was engaged in organic LED technology for thin-film display applications. He is currently a Postdoctoral Researcher at the University of California, Berkeley, where his research involves light–matter interactions in subwavelength optical nanocavities and plasmonics.

Xiang Zhang received the B.S. and M.S. degrees in solid-state physics from Nanjing University, Nanjing, China, and the Ph.D. degree in mechanical engineering from the University of California, Berkeley.

He is currently a Chancellor's Professor and the Director of the National Science Foundation (NSF) Nanoscale Science and Engineering Center, University of California, Berkeley, where he is also a Professor of the Applied Science and Technology Program. His current research interests include plasmonics, metamaterials, nanomanufacturing, and devices.

Prof. Zhang was a recipient of the NSF Career Award (1997) and the Office of Naval Research Young Investigator Award (1999). He was the Chair of a session on Metamaterials, Quantum Electronics and Laser Science Conference (QELS 2006), Long Beach, CA, and the Technical Program, IEEE 2nd International Conference on Micro and Nano Engineered and Molecular Systems, Bangkok, Thailand, Jan. 2007.